Magnetic properties of co-ferrite nanoparticles prepared by co-precipitation method

M. Chithra[1,2,*], C. N. Anumol[1,3], V. Argish[1], B. N. Sahu[4], and Subasa C. Sahoo[1,*] (ID)

[1] *Department of Physics, Central University of Kerala, Tejaswini Hills, Periya, Kasaragod 671320, Kerala, India*

[2] *Department of Physics, E. K. Nayanar Memorial Government College, Elerithattu, P.O. Elerithattu, Kasaragod, Kerala 671314, India*

[3] *Department of Physics, Government College Kasaragod, Vidyanagar, Kasaragod, Kerala 671123, India*

[4] *Central Research Facility, Indian Institute of Technology Delhi, Hauz Khas, New Delhi 110016, India*

ABSTRACT

Co-ferrite nanoparticles were synthesised by coprecipitation method and were annealed at different temperatures in air. Grain size was observed to be increased with the increase in annealing temperature. Magnetisation value of the as-prepared sample was 57 emu/g at 300 K and increased with the increase in annealing temperature. The highest value of 76 emu/g was observed for the sample annealed at 900 °C. With the decrease in temperature to 60 K, it was enhanced from that at 300 K and the difference between the magnetisation values observed at 300 and 60 K, decreased with the increase in annealing temperature. The variation of coercivity showed a maximum of 1.02 kOe at 300 K for the nanoparticle sample with grain size of 27 nm. A very high value of energy product $(BH)_{max}$ of 5.6 MGOe was observed at 60 K for the sample annealed at 900 °C. Both exchange and dipolar interactions were observed in these nanoparticles. The nonsaturation behaviour of magnetic hysteresis loop decreased with the increase in grain size and annealing temperature. The observed magnetic properties can be correlated to grain size, surface defects, anisotropy and interparticle interactions in these nanoparticles.

1 Introduction

Spinel ferrites are an important class of magnetic oxides due to their potential technological applications in various fields. These ferrites have spinel crystal structure (MFe_2O_4) with O^{2-} ions forming closed packed fcc lattice and Fe^{3+} and M^{2+} cations occupy either tetrahedral (A) or octahedral (B) interstitial sites in the crystal structure. Among ferrites, Co-ferrite ($CoFe_2O_4$) has attracted much attention due to its high coercivity [1], anisotropy [2], magnetostriction [3], Curie temperature [4] and magnetisation [5]. In bulk Co-ferrite, all the 8 Co^{2+} ions occupy the B-sites and 16 Fe^{3+} ions are distributed equally in both A and B-sites in the unit cell. In nanoscale, these nanoparticles show different

Address correspondence to E-mail: chithragovindm@gmail.com; subasa.cs@gmail.com

Ⓐ Springer

physical properties compared to the bulk. Hence the research on various properties of Co-ferrite nanoparticles is intensively going on for a better understanding of the size effects in these nanoparticles. Žalnėravičius et al. studied size dependent antimicrobial properties of Co-ferrite nanoparticles [6]. Arunkumar et al. observed a semiconducting to metallic phase transition in these nanoparticles with the decrease in size from 52 to 6 nm [7]. Influence of grain size and annealing temperature on the magnetic and magnetorheological properties were investigated by Sedlacik et al. [8]. Apart from these, synthesis methods also play crucial role in deciding the properties of these nanoparticles. Various synthesis methods like coprecipitation [9], sol–gel [10], microemulsions [11], polyol [12], hydrothermal [13], thermal decomposition [14] methods have been adopted to prepare ferrite nanoparticles. Coprecipitation methods is a cost effective and simpler method in the wet chemical methods [9]. In this work, we prepared Co-ferrite nanoparticles by coprecipitation method and studied the effect of annealing on its structural and magnetic properties including the non-saturation behaviour of the magnetic hysteresis loops of these nanoparticles.

2 Experimental details

Co-ferrite nanoparticles were synthesized using coprecipitation method. In the synthesis process, 1 M (25 ml) solution of iron chloride ($FeCl_3$) and 0.5 M (25 ml) solution of cobalt chloride ($CoCl_2 \cdot 6H_2O$) were prepared in separate beakers with double distilled deionized water. The salt solutions were mixed together under constant stirring at room temperature. Solution of sodium hydroxide (NaOH) of 3 M was slowly added to the metal salt solution drop wise to reach pH of 12. The solution was kept under constant stirring at 80 °C and a black color precipitate was formed uniformly in the solution. After 2 h, it was cooled down to room temperature. The precipitate was washed several times with distilled water. By centrifuging at 6000 rpm for 30 min, the precipitate was collected from the supernatant liquid and was dried overnight at 150 °C. This sample was ground well and is designated as the as-prepared sample. The as-prepared powder was annealed at different temperatures (T_A) up to 900 °C in air for 2 h and was cooled down to room temperature inside the furnace.

The structural properties were studied by X-ray diffraction (XRD) by a Rigaku Miniflex 600 X-ray diffractometer with Cu-K$_\alpha$ radiation ($\lambda = 1.5406$ Å) in $\theta/2\theta$ mode. Microstructure of the samples was obtained by a Carl Ziess Sigma field emission gun scanning electron microscope (FEG-SEM) and high resolution transmission electron microscope (HRTEM) JEOL JEM-2100. Magnetic measurements were carried out in the temperature range 310 to 50 K by a vibrating sample magnetometer of Quantum Design Versa Lab Physical Property Measurement System by applying maximum magnetic field up to ± 30 kOe.

3 Results and discussion

Figure 1 shows the XRD patterns of the as-prepared and the annealed Co-ferrite nanoparticles. All the observed peaks were indexed to the cubic spinel Co-ferrite. The lattice constant and grain size were calculated using the most intense peak and are shown in Table 1. As seen from the Table 1, the lattice constant does not show any systematic variation with the increase in T_A and was found to be in the range of 8.332–8.389 Å which are always less than the bulk value of 8.391 Å. As seen in the Fig. 1, with the increase in T_A, the diffraction peaks became narrower indicating grain growth in these samples. The grain size of the as-prepared sample was 17 nm as shown in Table 1 and it increased monotonically with the
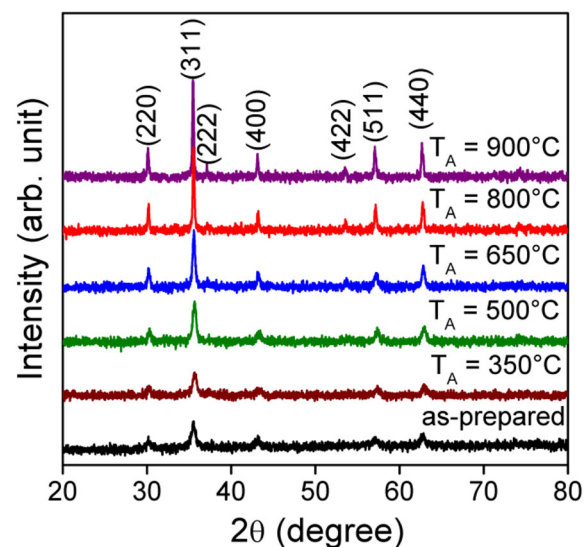
Fig. 1 XRD patterns of the Co-ferrite nanoparticles annealed at different temperatures

Table 1 Lattice constant and grain size of the Co-ferrite nanoparticles

T_A (°C)	Lattice constant (Å)	Grain size (nm)
As-prepared	8.379	17.4
350	8.342	15.8
500	8.349	19.0
650	8.366	26.6
800	8.374	42.5
900	8.389	46.9

increase in T_A and reached a maximum value of 47 nm for the sample annealed at T_A = 900 °C.

The SEM images of the as-prepared and the annealed (T_A = 900 °C) Co-ferrite nanoparticles are shown in Fig. 2a and b. As seen in Fig. 2a and b the grains were small and spherical in size for the as-prepared sample and were increased after annealing. Figure 2c shows the TEM image of the as-prepared Co-ferrite nanoparticles and the grain size distribution of these sample is shown in the inset. It is seen in the Fig. 2c that the grains are very small in size for the as-prepared sample as observed by XRD and SEM. Moreover, there is no aglomeration in the nanoparticle sample. All the observed diffraction rings in the selected area electron diffraction (SAED) pattern were identified and the rings were indexed as shown in Fig. 2d.

Figure 3 shows the magnetic hysteresis (M-H) loops of the as-prepared and the annealed samples. As seen in the Fig. 3, the M–H loops were not saturated up to the maximum applied field of 30 kOe. To obtain the magnetization value (M_S), the high field part of the loop was extrapolated to the zero applied fields [10, 15, 16]. The M_S values obtained from the loops are shown in Fig. 4 as a function of T_A. The M_S value of the as-prepared sample was 57 emu/g at 300 K and was slightly decreased to 55 emu/g with the increase in T_A to 350 °C as seen in Fig. 4a. With further increase in T_A, the M_S value started increasing continuously. A maximum value of 76 emu/g was observed at 300 K for the sample annealed at 900 °C. The maximum observed value is 5% lower than the bulk value of 80 emu/g [17]. Prabakaran et al. reported a continuous increase of M_S value with the increase in T_A for the nanoparticles synthesized by the coprecipitation method; however they observed a maximum value of 59 emu/g at T_A = 800 °C [18]. Monotonic increase in the M_S value with the increase

in annealing temperature and grain size has also been reported by other groups [19, 20]. It is also seen from Fig. 4a that, with the decrease in measurement temperature to 60 K, the M_S value was increased from 57 to 67 emu/g for the as-prepared sample and followed similar trend with the increase in T_A as observed at 300 K. Moreover, the difference in the magnetization values ΔM_S, where ΔM_S = M_S(60 K)−M_S(300 K), decreased with the increase in T_A as seen in Fig. 4b.

As seen in the Fig. 4c, the M_r/M_S ratio of 0.34 was observed for the as-prepared sample at 300 K and was increased with the increase in T_A; showed a maximum value of 0.47 at T_A = 650 °C and then slightly decreased with the further increase in T_A. At lower temperature of 60 K, the M_r/M_S ratio increased for all these samples. However, the value remained constant in the annealed samples.

The coercivity (H_C) increases with the increase in grain size as shown in Fig. 4d both at 300 K and 60 K; reached a maximum value and then decreases with further increase in grain size. The maximum H_C of 1.02 kOe was observed at 300 K for the nanoparticles with grain size $\approx$ 27 nm. Both above and below this critical size the H_C decreases. Toksha et al. observed a maximum H_C of 1.21 kOe in the Co-ferrite nanoparticles with grain size of 25 nm, prepared by sol–gel auto combustion method [20]. Sudheesh et al. observed a maximum H_C of 1.13 kOe in the Co-ferrite nanoparticles with grain size of 60 nm prepared by sol–gel method [21]. Chinnasamy et al. also observed similar trend of grain size dependence of H_C and observed a maximum value of 4.65 kOe for the sample with grain size of 40 nm [1]. A monotonic increase of H_C was observed for the Co-ferrite nanoparticles with grain size ($\leq$ 27 nm) [18] and a decrease of H_C with increase in grain size ($\geq$ 30 nm) was also reported [8]. However, a continuous decrease in H_C from 4.7 to 1.2 kOe with increase in grain size from 13 to 114 nm was also reported [22]. With the decrease in temperature from 300 K to 60 K, very high value of H_C, even one order higher than that at 300 K, was observed as seen in Fig. 4d. The variation of H_C at 60 K with T_A followed the similar pattern that was observed at 300 K. However, the peak in H_C was shifted to lower grain size of 19 nm with the value of 13.66 kOe.

The observed magnetic behaviour in these nanoparticles can be explained as follows. In nanoparticles, size and surface effects dominate the magnetic properties. The magnetic moments are
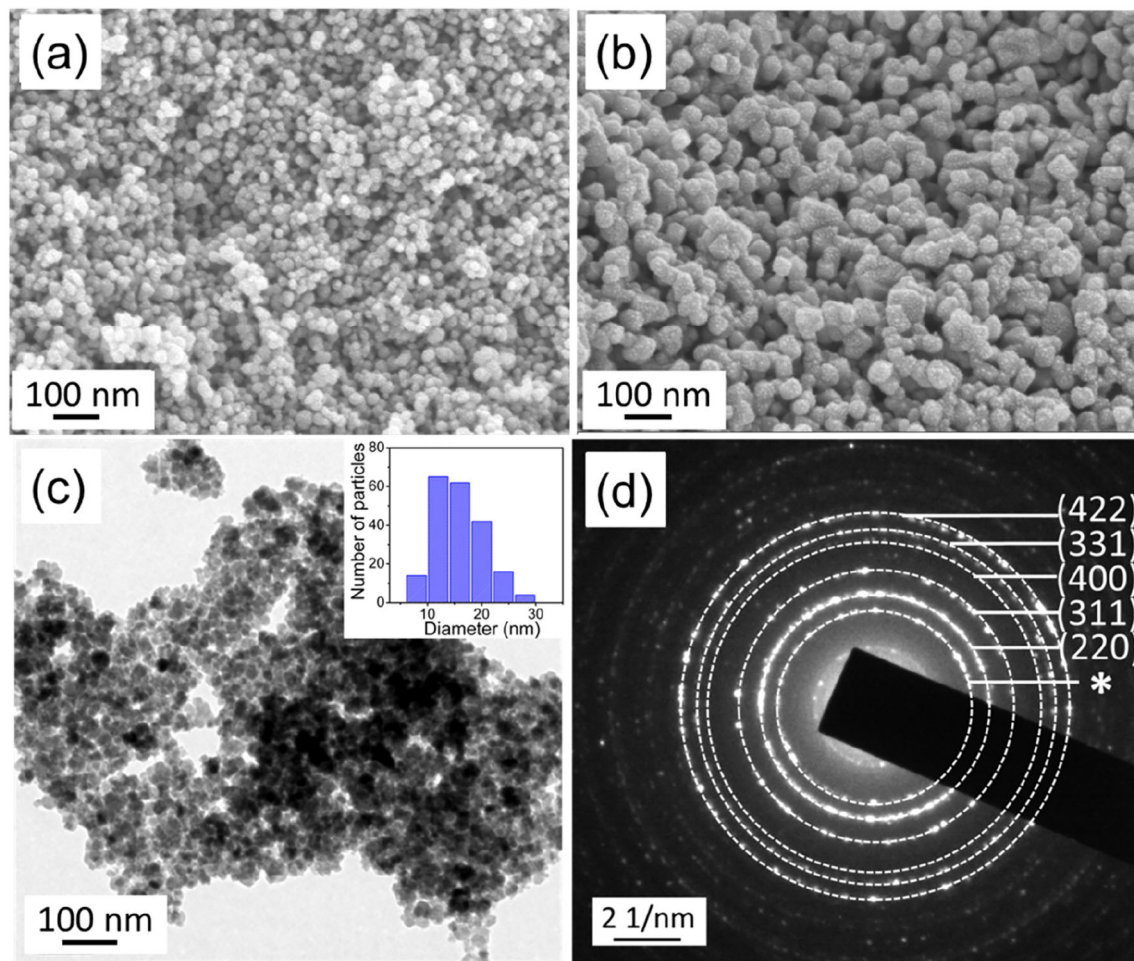
Fig. 2 SEM images of **a** the as-prepared and **b** the annealed (T_A = 900 °C) Co-ferrite nanoparticles; **c** TEM image (grain size distribution is shown in the inset) and **d** SAED pattern of the as-prepared Co-ferrite nanoparticles (*corresponds to CuO phase coming from the copper grid used in the TEM sample preparation)

canted at the surface of the nanoparticles due to the defects while in the core they are ordered. The surface contribution is higher in the nanoparticles compared to the volume contribution. Hence the net magnetization in the nanoparticles is observed to be less than that of the bulk [10]. As the grain size increases after annealing, the surface effects decrease; as a result magnetization increases in these nanoparticle samples. When the measurement temperature decreases to 60 K, the thermal energy decreases; the spin-orbit coupling becomes stronger. As a result magnetisation increases in the samples. The initial decrease in the M_S value for the sample annealed at T_A = 350 °C, from that observed for the as-prepared sample, as seen Fig. 4a may be understood as follows. It is quite possible that in the as-prepared sample, there may be some unreacted

Co^{2+}/Fe^{3+} ions or metal complex present in the grain boundary region of the nanoparticles. With the increase in T_A these unreacted Co^{2+} and Fe^{3+} ions reacted with O_2 to form spinel $CoFe_2O_4$. The magnetic moments are antiparallel to each other in the two magnetic sub-lattices in the A and B-sites in the spinel structure. So, the magnetization decreased for the sample annealed at T_A = 350 °C. The enhancement of M_S value at 60 K from that at 300 K, (i.e. ΔM_S) decreases with the increase in T_A as mentioned earlier. There are grains of different sizes distributed in the nanoparticle samples. With the decrease in measurement temperature, stronger spin-orbit coupling favours the enhancement of magnetization. At the same time, magnetic moments are blocked at random direction in some nanoparticles. Moreover, strong dipolar interaction between the
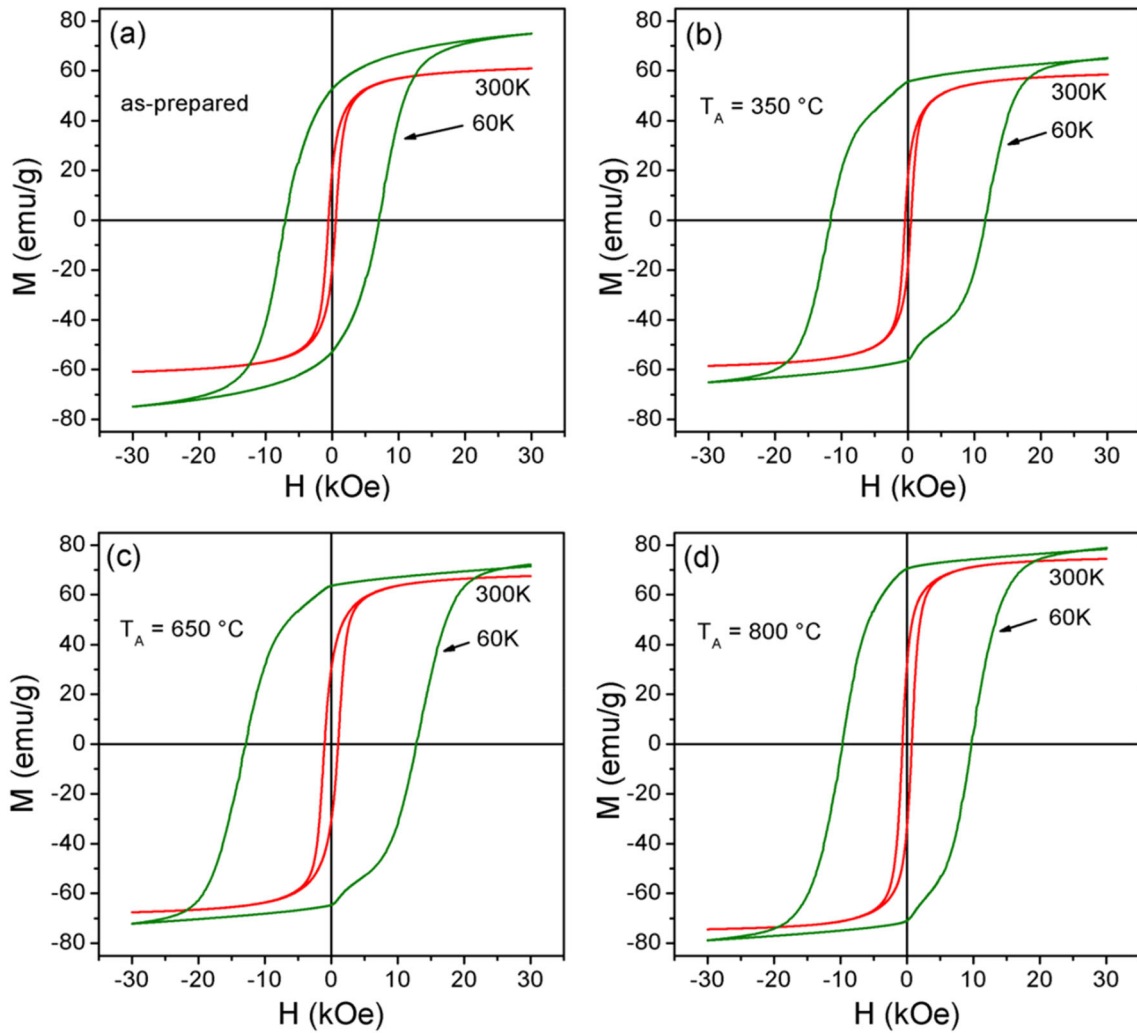
Fig. 3 M-H loops of the as-prepared and the annealed Co-ferrite nanoparticles

superparmagnetic grains in the blocked state forbids the moments to align along the field direction in these nanoparticle samples [10]. Competition between these factors results decrease in ΔM_S value with the increase in T_A.

The coercivity (H_C) depends on many factors like grain size, anisotropy, cation distribution, intergranular interaction, microstructure, and domain structure. In the present study the behavior of H_C can be understood as follows. From the Fig. 4d, it is inferred that the critical single domain grain size is 27 nm in these Co-ferrite nanoparticles. As the grain size is lower than the critical size the anisotropy decreases and so does the H_C. After the critical size, formation of multi domains lowers the H_C. With the decrease in temperature to 60 K, the effective anisotropy and H_C increased. However, the peak was shifted to lower

grain size of 19 nm. With the decrease in temperature, the surface anisotropy in addition to the size of the grains plays significant role in smaller grains [23, 24].

The maximum energy product $(BH)_{max}$ is the figure of merit for the permanent magnet applications [2]. We have evaluated the $(BH)_{max}$ value for these Co-ferrite nanoparticles and tried to understand the various factors affecting this parameter. The plot of BH versus H is shown in Fig. 5a and the maximum value as indicated by an arrow in the graph, is the $(BH)_{max}$ for the sample. Figure 5b shows the variation of $(BH)_{max}$ with respect to annealing temperature (T_A) at 300 and 60 K. It is interesting to see that $(BH)_{max}$ shows a similar variation with respect to T_A as that of H_C at 300 K. At 300 K, as T_A increases, $(BH)_{max}$ increases and reaches a maximum value of
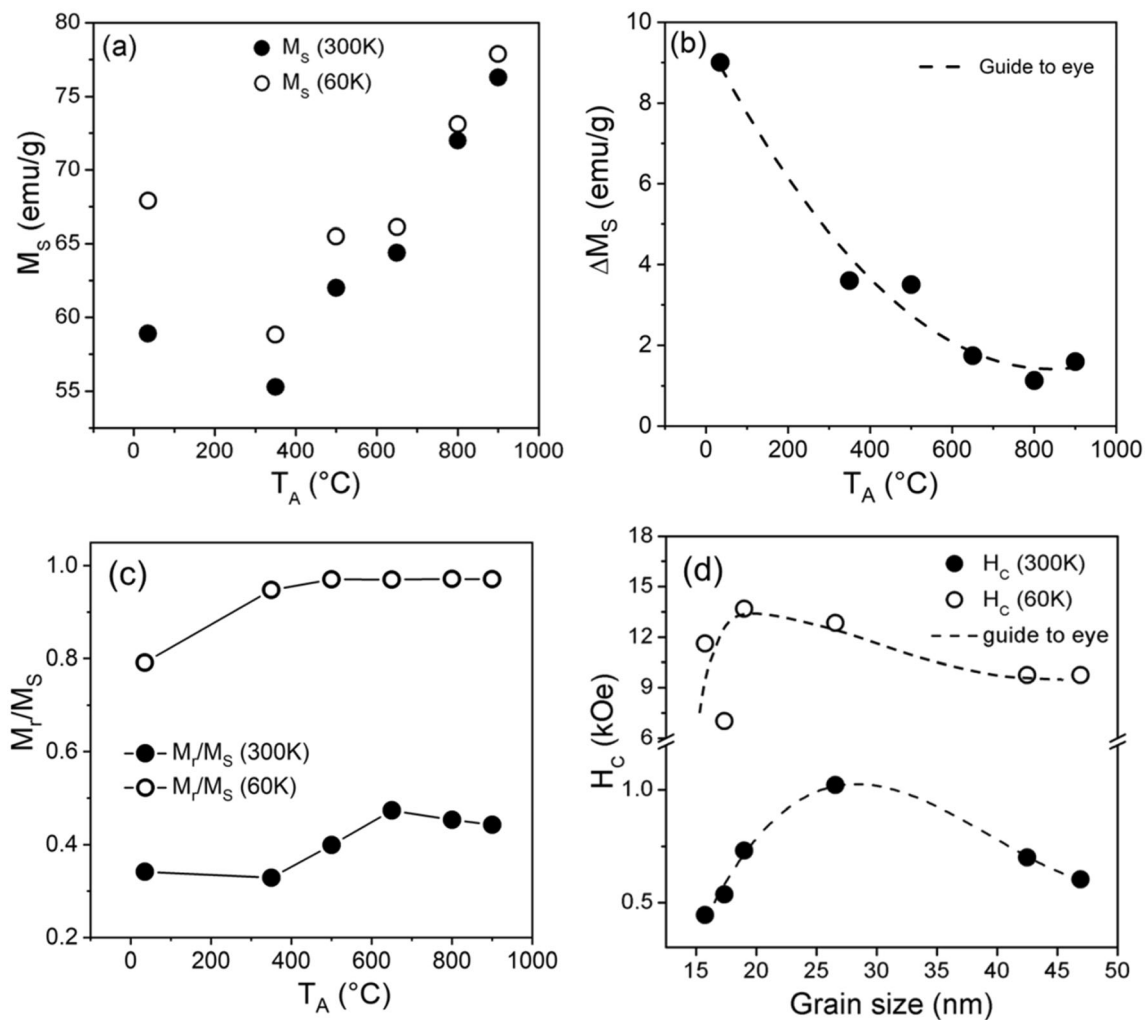
Fig. 4 Variation of **a** M_S, **b** ΔM_S, **c** M_r/M_S with T_A and **d** H_C with grain size for the Co-ferrite nanoparticles

0.42 MGOe for the sample annealed at 650 °C and then decreases with further increase in T_A. Similar behavior is also reported in literatures [22, 25, 26]. Kumar et al. reported the highest $(BH)_{max}$ value of 2.4 MGOe at 300 K for Co-ferrite nanoparticles with grain size of 35 nm [26]. With the decrease in measurement temperature from 300 K to 60 K, a drastic increase in the $(BH)_{max}$ value was observed as depicted in Fig. 5b. Moreover, unlike the variation at 300 K, the $(BH)_{max}$ value continuously increases with the increase in T_A at 60 K and a very high value of 5.6 MGOe was observed for the sample annealed at 900 °C.

The energy product $(BH)_{max}$ of a material is related to its H_C and M_r/M_S ratio or how rectangular is the shape of the demagnetization curve of the hysteresis loop [25]. In our samples, it seems like H_C strongly influences the behavior of $(BH)_{max}$ at 300 K. However

at 60 K, the high values of H_C as well as M_r/M_S resulted in very high value of $(BH)_{max}$ and an interplay between these two factors might have resulted in continuous increase in the $(BH)_{max}$ value with the increase in T_A.

In order to understand the inter-granular interaction in these nanoparticles as it influences the magnetic properties, we have carried out the δM measurements to study the effect of T_A and grain size on it. The isothermal remanent magnetization (IRM) [$M_r(H)$] and DC demagnetization remanence (DCD) [$M_d(H)$] curves were measured at 300 and 60 K up to 30 kOe. For IRM measurement, the sample is totally demagnetized and cooled to the required temperature in zero applied magnetic fields. A small positive external field (H) is applied for certain period of time and switched off, and then the remanence $M_r(H)$ is measured. This process is repeated by increasing the
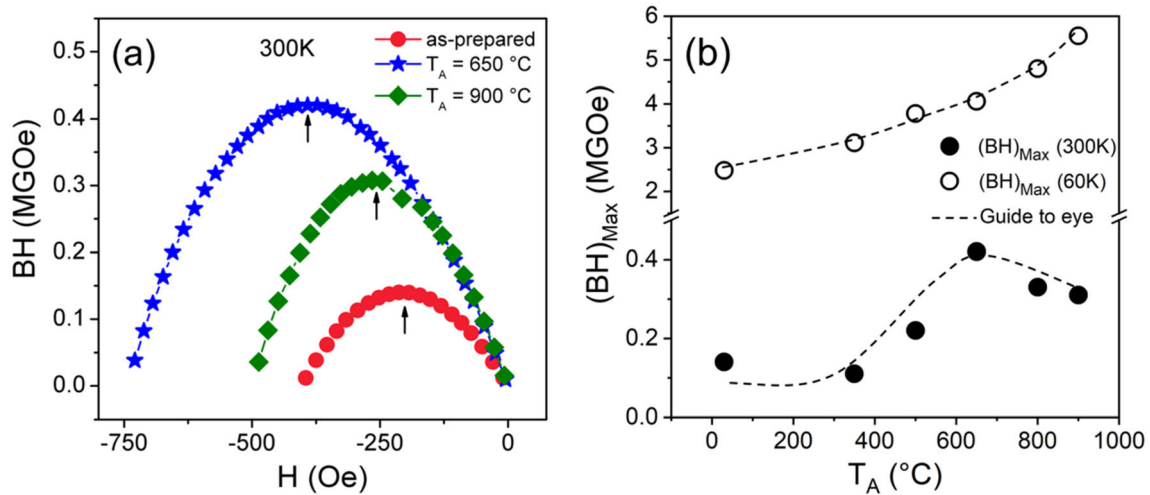
Fig. 5 a The energy product curves at 300 K for the as-prepared and annealed samples and the $(BH)_{Max}$ values are indicated by the arrows in the figure, **b** Variation of $(BH)_{Max}$ as a function of T_A

magnitude of H until the sample reaches saturation and the remanence at saturation is $M_r(\infty)$. In the measurement of DC demagnetization, the sample is initially at saturated state at a particular temperature. A small external magnetic field (H) is applied in a direction opposite to the magnetization and is switched off after sometime, and $M_d(H)$ is measured. This is repeated by increasing H until the saturation in the opposite direction is attained. Same values of H are used in both procedures. In our experiment the maximum applied field available was 30 kOe and the highest IRM and DCD magnetizations obtained were M_r (30 kOe) and M_d(30 kOe) respectively. The two remanence curves, are related by Wohlfarth equation established for the noninteracting single domain uniaxial nanoparticles as [27, 28],

$$m_d(H) = 1 - 2m_r(H)$$

where $m_r(H)$ and $m_d(H)$ are the reduced magnitudes of IRM and DCD with remanence saturation values; i.e., $m_r(H) = M_r(H)/ M_r(30kOe)$ and $m_d(H) = M_d(-H)/M_r(30kOe)$ in our case. Any deviation from this straight line equation is an indication of interparticle interaction among the nanoparticles [27–30]. The strength of the interaction can also be quantified by δM given by the equations [27, 28] as,

$$\delta M = m_d(H) - [1 - 2m_r(H)]$$

A positive deviation i.e., if the deviation is above the linear behavior suggests the presence of magnetizing exchange interactions and a negative deviation i.e., below the linear behavior suggests demagnetizing dipolar interactions.

Figure 6 shows the δM curves for the as-prepared and the annealed (T_A = 900 °C) samples. As seen in Fig. 6, a negative peak was observed for the as-prepared sample. However, for the sample annealed at T_A = 900 °C, the peaks were observed both in positive and negative directions. Moreover, the amplitude of the negative peak in the annealed sample is higher than that observed for the as prepared sample. In general, observation of negative peak in the δM curve shows dominant dipolar interaction, and the positive peak attributed to the dominant exchange interactions in the nanoparticles [31]. As the grain size increases and surface to volume ratio decreases with the increase in T_A, magnetic dipolar interaction increases. That is the reason for the increase in amplitude of δM curves with the increase in T_A. At lower temperature, the strength of the dipolar interaction increases with stronger spin-orbit coupling, as the thermal energy decreased. At the same time anisotropy also increases with the decrease in thermal energy. Anisotropy in the sample opposes the interparticle interaction. The magnetic moments in the nanoparticles couple with each other by exchange interaction [32] in addition to the dipolar interaction in the annealed samples which resulted appearance of more peaks. Our study clearly shows that the strength and type of interactions in the Co-ferrite nanoparticles depend on the surface layer thickness, spin-orbit coupling strength, anisotropy and grain size in the sample.
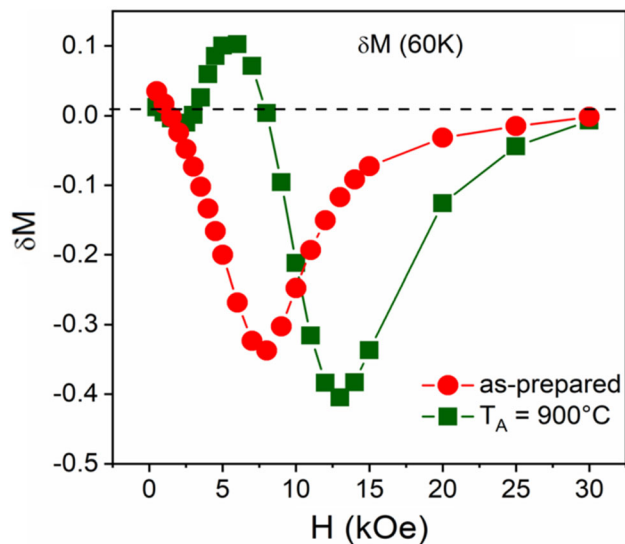
Fig. 6 δM curves for the as-prepared and annealed Co-ferrite nanoparticles at 60 K

As we have seen earlier, the M-H loops were not saturated even at high field of 30 kOe. The non-saturation behaviour of the ferrite nanoparticles has been reported by many researchers [15, 33–35]. The non-saturation behaviour of the M-H loops depends on various factors like spin canting, cation distribution [36], presence of super paramagnetic grains [35], anisotropy [24, 37] and surface defects [38]. In the nanoparticles point defects and magnetic anisotropy at the atomic scale dominate the non-saturation behaviour and is best described by the equation $M(H) = M(\infty)\left[1 - \sqrt{\frac{H^*}{H}}\right]$, where $M(\infty)$ is the magnetization at infinite field and H^* gives the qualitative information about the non-saturation [15]. We fitted our data in the high field region of the initial curve between 20 and 30 kOe to the above equation. The fitted curves for the as-prepared and the annealed Co-ferrite nanoparticles are shown in Fig. 7a. As seen in Fig. 7a the equation is best fitted to our experiment data. The values of $M(\infty)$ and H^* obtained from the fitting were plotted as function of T_A and are shown in Fig. 7b. As seen in Fig. 7b, the $M(\infty)$ value increases with the increase in T_A similar to the variation of M_S value with the increase in T_A. The H^* value decreases with the increase in T_A at 300 K, i.e., the loops show better saturation with the increase in T_A. With the increase in T_A, grain size is increased in these samples as mentioned above. The decrease in

surface defects with the increase in T_A leads to better saturation in these samples.

Figure 8 shows the variation of magnetization in the ZFC (M_{ZFC}) mode and FC mode (M_{FC}) with temperature for the Co-ferrite nanoparticles. As seen in Fig. 8a, the M_{ZFC} increases continuously with increase in temperature from 50 to 310 K whereas M_{FC} slowly decreases with the increase in temperature for the as-prepared sample. The M_{FC} is found to be higher than M_{ZFC} and never meet M_{ZFC} in this temperature range. The sample annealed at 900 °C show similar behavior. A hump was observed around ≈ 156 K in the ZFC curve of the annealed sample.

In the magnetic nanoparticles, initially the magnetic moments are randomly frozen at low temperature. When a certain field is applied, the magnetic moments are unable to align along the field direction due to high anisotropic energy barrier at low temperature. As the temperature increases, magnetic moments are freed from the anisotropy energy barrier and are aligned along the field direction. So, the magnetization increases with the increase in temperature in the ZFC magnetization curve. When most of the moments are aligned in the field direction, a maximum is observed in the ZFC curve at a particular temperature known as blocking temperature (T_B). After T_B, the thermal energy overcomes the anisotropy energy barrier, and the moments try to align at random, showing a transition from the ordered state to a disordered state, i.e., from ferrimagnetic to superparamagnetic state. It seems that the T_B is above 310 K for the as-prepared sample. The T_B is affected by the grain size [39] and their distribution [40], interparticle interaction, anisotropy [41], cooling and heating rate during the magnetic measurement [42]. For the sample annealed at 900 °C, it seems that there are two transitions; one around ≈ 156 K and another one above 310 K. In FC measurement, the magnetic moments have been aligned in a particular direction as the sample was cooled in presence of the field and the magnetization decreases due to the relaxation of moments with the increase in temperature.
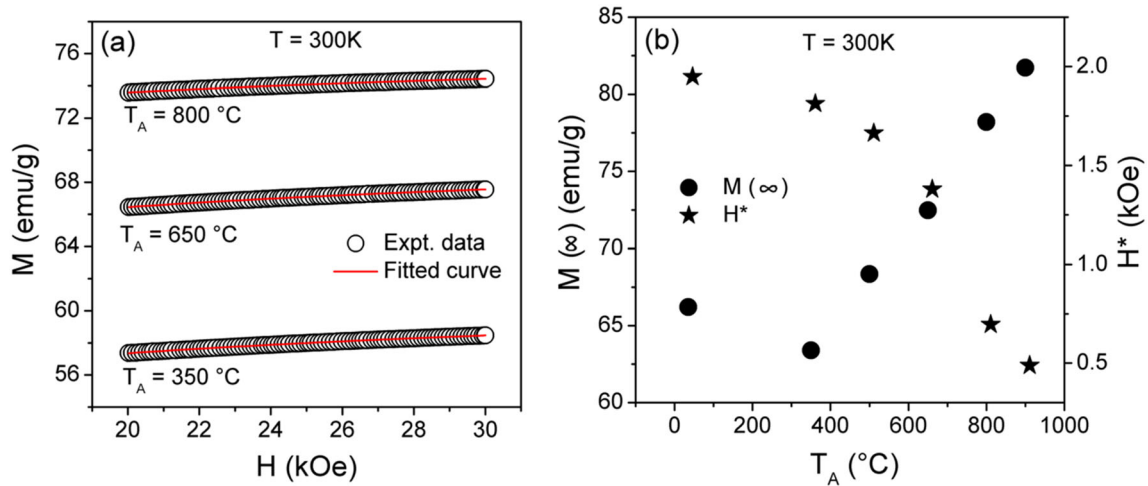
Fig. 7 a Fitting to high field part of the virgin curves for the annealed Co-ferrite nanoparticles with the equation $M(H) = M(\infty)\left[1 - \sqrt{\frac{H^*}{H}}\right]$, **b** Variation of $M(\infty)$ and H^* with T_A
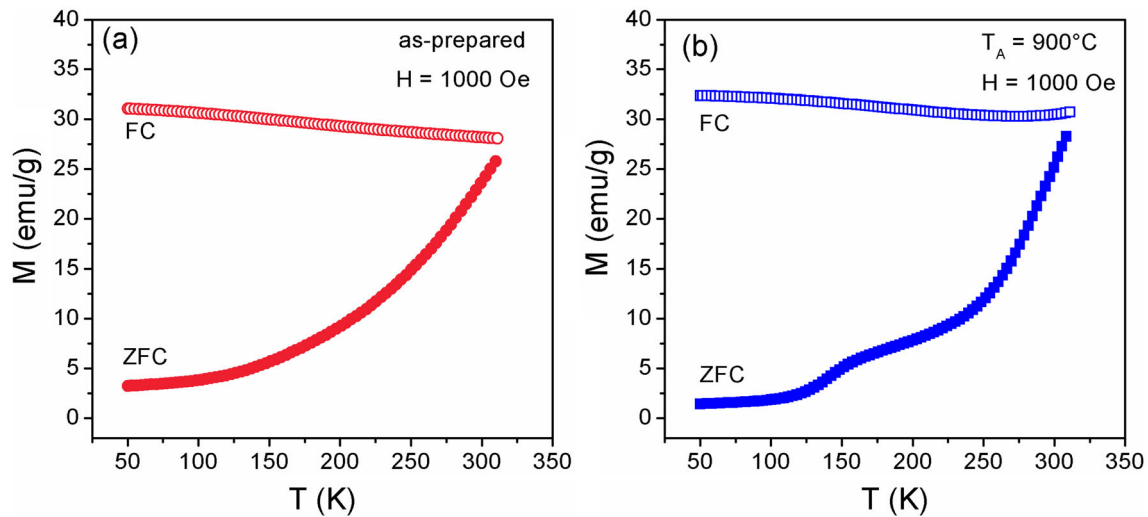
Fig. 8 ZFC-FC curves of the **a** as-prepared and **b** the annealed ($T_A = 900$ °C) Co-ferrite nanoparticles prepared by coprecipitation method

4 Conclusion

Co-ferrite nanoparticles were synthesized using coprecipitation method and were annealed at different temperatures for 2 h in air. The grain size was observed to be increased from 17 nm to a maximum value of 47 nm with the increase in T_A. The magnetization value increased with the increase in T_A and the highest M_S value of 76 emu/g was observed at 300K for the nanoparticle sample annealed at 900°C and a very high value of energy product $(BH)_{max}$ of 5.6 MGOe was observed at 60K for the same sample. The variation of coercivity with grain size showed a maximum for the critical single domain grain size of

27 nm. Both exchange and dipolar interactions were observed in these nanoparticle samples in δM measurements. The non-saturation of magnetic hysteresis loops decreased with the increase in grain size and T_A. The observed magnetic properties can be attributed to the grain size, surface defects, anisotropy, and interparticle interactions in these nanoparticles.

Author contributions

MC–Conceptualization, data curation, formal analysis, investigation, writing of original draft, CNA—

data curation, investigation, VA—data curation, investigation, BNS—data curation, investigation, formal analysis, writing—review & editing, SCS—Conceptualization, formal analysis, validation, supervision, writing—review & editing. All authors commented on previous versions of the manuscript. All authors read and approved the final manuscript.

Funding

Data availability

The datasets generated during and/or analysed during the current study are available from the corresponding author on reasonable request.

Research data policy

https://doi.org/10.6084/m9.figshare.21770483

Declarations

Conflict of interest The authors have no relevant financial or non-financial interests to disclose.

References

1. C.N. Chinnasamy, B. Jeyadevan, K. Shinoda, K. Tohji, Appl. Phys. Lett. **83**, 2862 (2003)
2. A. López-Ortega, E. Lottini, C.D.J. Fernández, C. Sangregorio, Chem. Mater. **27**, 4048–4056 (2015)
3. J. Wang, X. Gao, C. Yuan, J. Li, J. Magn. Magn. Mater. **401**, 662–666 (2015)
4. A. Franco, F.C. Silva, Appl. Phys. Lett. **96**, 172505 (2010)
5. Y.C. Wang, J. Ding, J.H. Yin, B.H. Liu, J.B. Yi, S. Yu, J. Appl. Phys. **98**, 124306 (2005)
6. R. Žalnėravičius, A. Paškevičius, M. Kurtinaitiene, A. Jagminas, J. Nanoparticle Res. **18**, 300 (2016)
7. A. Arunkumar, D. Vanidha, K. Oudayakumar, S. Rajagopan, R. Kannan, J. Appl. Phys. **114**, 183905 (2013)
8. M. Sedlacik, V. Pavlinek, P. Peer, P. Filip, Dalton Trans. **43**, 6919–6924 (2014)
9. T. Prabhakaran, R.V. Mangalaraja, J.C. Denardin, J.A. Jimenez, Ceram. Int. **43**, 5599–5606 (2017)
10. M. Chithra, C.N. Anumol, B. Sahu, S.C. Sahoo, J. Magn. Magn. Mater. **401**, 1–8 (2016)
11. S. Li, V.T. John, J. Appl. Phys. **87**, 6223–6225 (2000)
12. M. Artus, L.B. Tahar, F. Herbst, L. Smiri, F. Villain, N. Yaacoub, J.-M. Grenèche, S. Ammar, F. Fiévet, J. Phys. Condens. Matter **23**, 506001 (2011)
13. Y. Zhang, Y. Liu, Z. Yang, R. Xiong, J. Shi, J. Nanoparticle Res. **13**, 4557 (2011)
14. Y. Kumar, P.M. Shirage, J. Mater. Sci. **52**, 4840–4851 (2017)
15. M. Chithra, C.N. Anumol, B. Sahu, S.C. Sahoo, J. Magn. Magn. Mater. **424**, 174–184 (2017)
16. M. Chithra, C.N. Anumol, V. Argish, B. Sahu, S.C. Sahoo, J. Mater. Sci. Mater. Electron. **29**, 813–822 (2018)
17. B.D. Cullity, C.D. Graham, *Introduction to Magnetic Materials*, Second edn. (John Wiley and Sons, INC, 2009)
18. T. Prabhakaran, R.V. Mangalaraja, J.C. Denardin, J.A. Jimenez, J. Alloys Compd. **716**, 171–183 (2017)
19. F. Huixia, C. Baiyi, Z. Deyi, Z. Jianqiang, T. Lin, J. Magn. Magn. Mater. **356**, 68–72 (2014)
20. B.G. Toksha, S.E. Shirsath, S.M. Patange, K.M. Jadha, Solid State Commun. **147**, 479–483 (2008)
21. V.D. Sudheesh, N. Thomas, N. Roona, P.K. Baghya, V. Sebastian, Ceram. Int. **43**, 15002–15009 (2017)
22. F.J. Pedrosa, J. Rial, K.M. Golasinski, M. Rodriguez-Osorio, G. Salas, D. Granados, J. Camarero, A. Bollero, RSC Adv. **6**, 87282–87287 (2016)
23. S.T. Xu, Y.Q. Ma, G.H. Zheng, D.X. Dai, Nanoscale **7**, 6520–6526 (2015)
24. K.A. Mozul, L.P. Ol'khovik, Z.I. Sizova, A.N. Bludov, V.A. Pashchenku, V.N. Baumer, V.V. Vashchenko, M.O. Kolosov, A.P. Kryshtal, M.F. Prodanoy, Low Temp. Phys. **39**, 365–369 (2013)
25. B. Abraime, A. Mahmoud, F. Boschini, M.A. Tamerd, A. Benyoussef, M. Hamedoun, Y. Xiao, A. El Kenz, O. Mounkachi, J. Magn. Magn. Mater. **467**, 129–134 (2018)
26. Y. Kumar, A. Sharma, M.A. Ahmed, S.S. Mali, C.K. Hong, P.M. Shirage, New J. Chem. **42**, 15793–15802 (2018)
27. E.P. Wohlfarth, J. Appl. Phys. **29**, 595–596 (1958)
28. J. Garcia-Otero, M. Porto, J. Rivas, J. Appl. Phys. **87**, 7376 (2000)
29. J.M. Soares, F.A.O. Cabral, J.H. Araújo, F.L.A. Machado, Appl. Phys. Lett. **98**, 72502 (2011)
30. M. Kaur, J.S. McCloy, W. Jiang, Q. Yao, Y. Qiang, J. Phys. Chem. C **116**, 12875–12885 (2012)
31. S.T. Xu, Y.Q. Ma, Y.F. Xu, X. Sun, B.Q. Geng, G.H. Zheng, Z.X. Dai, Mater. Res. Bull. **62**, 142–147 (2015)
32. N.B. Herndon, S. Ho, Oh, J.T. Abiade, D. Pai, J. Sankar, S.J. Pennycook, D. Kumar, J. Appl. Phys. **103**, 075D515 (2008)

33. T.P. Sumangala, C. Mahender, N. Venkataramani, S. Prasad, J. Magn. Magn. Mater. **382**, 225–232 (2015)

34. J. Dash, S. Prasad, N. Venkataramani, R. Krishnan, P. Kishan, N. Kumar, S.D. Kulkarni, S.K. Date, J. Appl. Phys. **86**, 3303–3311 (1999)

35. P.D. Kulkarni, S. Prasad, N. Venkataramani, R. Krishnan, W. Pang, A. Guha, R.C. Woodward, R.L. Stamps, *Proceedings of the 9th International Conference on Ferrites (ICF-9)*, San Francisco, California, 2004, edited by R. F. Soohoo, Wiley (2005), p. 201

36. C.N. Chinnasamy, A. Narayanasamy, N. Ponpandian, K. Chattopadhyay, H. Guérault, J.-M. Greneche, J. Phys. Condens. Matter **12**, 7795–7805 (2000)

37. M. Bohra, S. Prasad, N. Venketaramani, N. Kumar, S.C. Sahoo, R. Krishnan, J. Magn. Magn. Mater. **321**, 3738–3741 (2009)

38. M. Bohra, V. Singh, M. Sowwan, J.-F. Bobo, C.-J. Chung, B. Clemens, J. Phys. D Appl. Phys. **47**, 305002 (2014)

39. N. Song, S. Gu, Q. Wu, C. Li, J. Zhou, P. Zhang, W. Wang, M. Yue, J. Magn. Magn. Mater. **451**, 793–798 (2018)

40. R. Malik, S. Annapoorni, S. Lamba, V.R. Reddy, A. Gupta, P. Sharma, A. Inoue, J. Magn. Magn. Mater. **322**, 3742–3747 (2010)

41. Y. Zhang, Y. Liu, C. Fei, Z. Yang, Z. Lu, R. Xiong, D. Yin, J. Shi, J. Appl. Phys. **108**, 084312 (2010)

42. V.N. Nikiforov, Y.A. Koksharov, S.N. Polyakov, A.P. Malakho, A.V. Volkov, M.A. Moskvina, G.B. Khomutov, V.Y. Irkhin, J. Alloys Compd. **569**, 58–61 (2013)